



**HAL**  
open science

# Arctic Curve of the Free-Fermion Six-Vertex Model in an L-Shaped Domain

F. Colomo, A. G Pronko, A. Sportiello

► **To cite this version:**

F. Colomo, A. G Pronko, A. Sportiello. Arctic Curve of the Free-Fermion Six-Vertex Model in an L-Shaped Domain. *Journal of Statistical Physics*, 2019, 174 (1), pp.1-27. 10.1007/s10955-018-2170-2 . hal-03205773

**HAL Id: hal-03205773**

**<https://hal.science/hal-03205773>**

Submitted on 22 Apr 2021

**HAL** is a multi-disciplinary open access archive for the deposit and dissemination of scientific research documents, whether they are published or not. The documents may come from teaching and research institutions in France or abroad, or from public or private research centers.

L'archive ouverte pluridisciplinaire **HAL**, est destinée au dépôt et à la diffusion de documents scientifiques de niveau recherche, publiés ou non, émanant des établissements d'enseignement et de recherche français ou étrangers, des laboratoires publics ou privés.

# Arctic curve of the free-fermion six-vertex model in an L-shaped domain

F. Colomo, A. G. Pronko, and A. Sportiello

ABSTRACT. We consider the six-vertex model in an L-shaped domain of the square lattice, with domain wall boundary conditions, in the case of free-fermion vertex weights. We describe how the recently developed ‘Tangent method’ can be used to determine the form of the arctic curve. The obtained result is in agreement with numerics.

## 1. Introduction

The thermodynamics of the six-vertex model with fixed boundary conditions has attracted much attention in recent years, in particular, as an example of a system exhibiting (in an appropriate scaling limit) spatial phase separation phenomena [1–12]. The model can be regarded as a nontrivial generalization of dimer models, and in particular, under specific geometry and boundary conditions, of the famous problem of domino tilings of the Aztec diamond, where the celebrated Arctic Circle phenomenon was discovered [13].

Among the many questions concerning this kind of effects, the shape of the phase separating curves (known as arctic curves) is of prime interest on its own right [14–29], and also in view of its relevance in relation with quantum quenches and nonequilibrium transport in one-dimensional quantum spin chains [9, 30, 31], and with spin-ice models [32].

In the case of the six-vertex model, within the various possible choices of fixed boundary conditions, domain wall boundary conditions [33] are the most studied. The arctic curve is known essentially only for the case of a square domain [5, 34, 35], although some recent progress has been made about the derivation of the arctic curve for the model in domains of more generic shape, from the knowledge of some suitable boundary correlation function, and of its asymptotic behaviour in the scaling limit [36].

In the present paper we consider the six-vertex model in an L-shaped domain. The partition function of the model has been evaluated in [37]. At the free-fermion point, it can be expressed as the partition function of some discrete log-gas [38, 39]. The corresponding free energy has been studied in [40, 41].

The analytic determination of the arctic curve of the model in an L-shaped domain, even only at the free-fermion point, is a nontrivial problem. In the free-fermion case, one could in principle use the general approach developed for dimer models in [18–20]. These papers establish the existence of the arctic curve, and its

analyticity, under general hypotheses which apply also here. They also provide a method for the analytic determination of the curve. However, while their method is quite amenable in the case of a triangular lattice (lozenge tilings), it becomes rather cumbersome for the square lattice (domino tilings).

Here, instead, we resort to the recently developed ‘Tangent method’ [36]. For this we need to calculate a suitable boundary correlation function of the six-vertex model in an L-shaped domain, and to estimate its asymptotic behaviour in the scaling limit. While most of the derivation can be carried out for generic choices of the Boltzmann weights, at the moment we are able to perform the aforementioned asymptotic evaluation only at the free-fermion point, the crucial limitation being the absence of an equivalent of the following Proposition 3.1 in the generic case.

The paper is organized as follows. We start by defining the model and introduce the correlation functions of interest for our purposes. Next we recall the Tangent method, which allows to determine the arctic curve from the knowledge of the asymptotic behaviour of some specific boundary correlation function. This is evaluated in terms of the so-called generalized emptiness formation probability (GEFP), introduced in [42], and expressed here, at the free-fermion point, in terms of the one-point correlation function of a discrete log-gas model. The asymptotic behaviour of the boundary correlation function is then evaluated, by resorting to standard techniques of random matrix models. Finally, using the Tangent method, the arctic curve of the model is obtained. We also show that the result is in excellent agreement with the numerical evaluation of the limit shape at finite size.

## 2. The six-vertex model on an L-shaped domain

In this section we recall basic facts about the six-vertex model with domain wall boundary conditions on an L-shaped domain. We define the GEFP, a rather general correlation function of the six-vertex model on the usual  $N \times N$  lattice with domain wall boundary conditions, which can be specialized to describe the partition function and some useful correlation functions in the case of the L-shaped domain. We formulate the problem of determination of the arctic curve arising in the scaling limit and set up some notation for parametrising the geometry of the domain.

**2.1. The lattice, configurations and weights.** The states of the six-vertex model are configurations of arrows pointing along the edges of a square lattice, and satisfying the condition that at each vertex the numbers of incoming and outgoing arrows are equal. This condition, known as *ice rule*, selects six possible vertex configurations. These are listed in Fig. 1, together with the corresponding Boltzmann weights,  $w_i$ ,  $i = 1, \dots, 6$ .

The L-shaped domain can be defined as a square domain with a rectangular portion removed from one of the corners, see Fig. 2a. Specifically, the square domain is the finite square lattice obtained from the intersection of  $N$  horizontal and  $N$

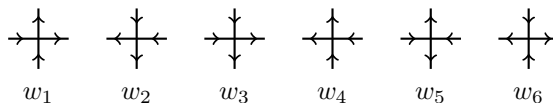


FIGURE 1. The six vertex configurations and their weights.

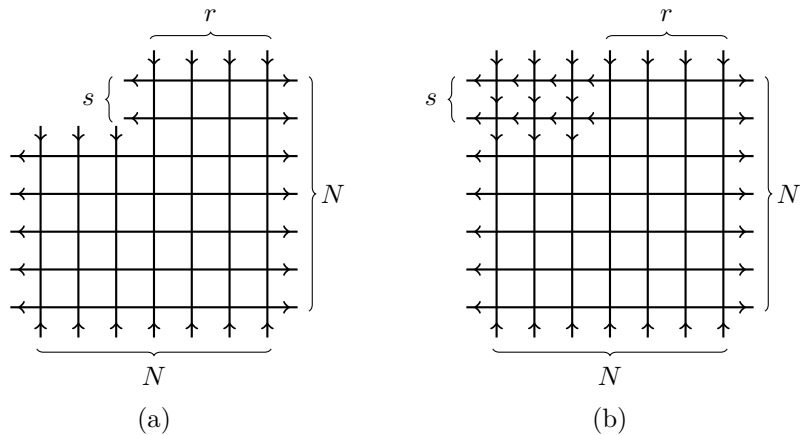


FIGURE 2. The L-shaped domain with domain wall boundary conditions: (a) The domain with a cut-off corner, (b) Equivalent arrow configuration on the original lattice. Here  $N = 7$ ,  $r = 4$ , and  $s = 2$ .

vertical lines (we will just say ‘the  $N \times N$  lattice’ for ‘the  $N \times N$  square domain of the square lattice’). The L-shaped domain is obtained by removing a rectangular portion of the lattice, of size  $s \times (N - r)$ , from the top-left corner of the square. The interesting range is  $r + s \leq N$  since otherwise there are no admissible arrow configurations.

For future convenience, we label the vertices of the square domain as follows: we associate the lattice coordinates  $(j, k)$  to the vertex at the intersection between the  $j$ th vertical line, counting from the right, and the  $k$ th horizontal line, counting from top. Correspondingly, the vertices of the L-shaped domain have labels  $(j, k)$ , with  $j = 1, \dots, r$  for  $k = 1, \dots, s$ , and  $j = 1, \dots, N$  for  $k = s + 1, \dots, N$ .

We impose domain wall boundary conditions by fixing all horizontal (respectively, vertical) arrows on external edges as outgoing (incoming). For  $s = 0$ , one has the usual  $N \times N$  lattice with domain wall boundary conditions, introduced in [33]. We denote the partition function of the six-vertex model in the L-shaped domain with domain wall boundary conditions by  $Z_{N,r,s}$ . When  $s$  or  $N - r$  is zero, we use the standard notation  $Z_N$ .

Under the choice of domain wall boundary conditions, due to the ice rule, there is an obvious correspondence between the six-vertex model on the L-shaped domain and the model on the  $N \times N$  square lattice, conditioned to have all vertex configurations of type 2 in the top-left  $s \times (N - r)$  rectangle, see Fig. 2b.

It is well known that (see, e.g., [6]), in presence of domain wall boundary conditions, one can restrict with no loss of generality to Boltzmann weights that are invariant under reversal of arrows, that is  $w_1 = w_2$ ,  $w_3 = w_4$ , and  $w_5 = w_6$ . In this paper we consider only the case in which they also obey the free-fermion condition  $w_1 w_2 + w_3 w_4 = w_5 w_6$ . In this case, and up to a global rescaling, one is left with a single real parameter, and we adopt the following parameterization of the Boltzmann weights:

$$w_1 = w_2 = \sqrt{1 - \alpha}, \quad w_3 = w_4 = \sqrt{\alpha}, \quad w_5 = w_6 = 1, \quad \alpha \in [0, 1]. \quad (2.1)$$

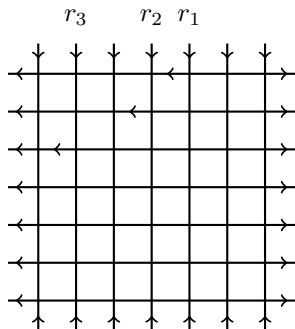


FIGURE 3. The configuration of arrows on the  $N \times N$  lattice, whose probability is described by the GEFP. Here  $N = 7$ ,  $s = 3$ , and  $(r_1, r_2, r_3) = (3, 4, 6)$ .

The construction above can be translated into the language of dimer models, using the well-known correspondence between the six-vertex model with domain wall boundary conditions and the domino tilings of the Aztec diamond [43]. The case of the six-vertex model on an  $N \times N$  square lattice with domain wall boundary conditions corresponds to the Aztec diamond of order  $N$ ; analogously, the model on the L-shaped domain corresponds to the Aztec diamond with a cut-off corner [40].

**2.2. The GEFP and boundary correlation function.** In [42], a rather general and flexible nonlocal correlation function, called *generalized emptiness formation probability* (GEFP), was introduced. For the six-vertex model on a square domain, it describes the probability of having an  $s$ -tuple of horizontal edges (one edge per line, in the first  $s$  horizontal lines, with corresponding column indices forming a weakly ordered sequence) all in a given state.

More precisely, enumerating the horizontal lines of the  $N \times N$  lattice from the top and the vertical lines from the right, we choose  $s$  edges,  $e_1, \dots, e_s$ ,  $1 \leq s \leq N$ , with edge  $e_k$ ,  $k = 1, \dots, s$ , located on the  $k$ th horizontal line, and between the  $r_k$ th and  $(r_k + 1)$ th vertical lines. We require the  $r_k$ 's to form a weakly increasing sequence  $1 \leq r_1 \leq \dots \leq r_s \leq N$ . We denote by  $G_{N,s}^{(r_1, \dots, r_s)}$  the probability of observing all arrows on the horizontal edges  $e_1, \dots, e_s$  to be pointing left, see Fig. 3a. Clearly, this is also the probability of having vertex configurations of type 2 at all sites  $(j, k)$  with  $r_k < j \leq N$ ,  $k = 1, \dots, s$ .

In [42] a multiple integral representation was derived for the GEFP (see equations (5.4) and (5.6) in that paper). Under the free-fermion condition and with parameterization (2.1), this representation reads

$$G_{N,s}^{(r_1, \dots, r_s)} = (-1)^s \oint_{C_0} \dots \oint_{C_0} \prod_{j=1}^s \frac{(\alpha z_j + 1 - \alpha)^{N-j}}{z_j^{r_j} (z_j - 1)^{s-j+1}} \prod_{1 \leq j < k \leq s} (z_j - z_k) \frac{d^s z}{(2\pi i)^s}. \quad (2.2)$$

In the special case  $r_1 = \dots = r_s = r$  the GEFP reduces to the usual emptiness formation probability (EFP) of the six-vertex model with domain wall boundary conditions, introduced in [34].

We emphasize that, although the GEFP has been defined for the model on a square domain, by suitably specializing the values of the  $r_j$ 's, it actually provides

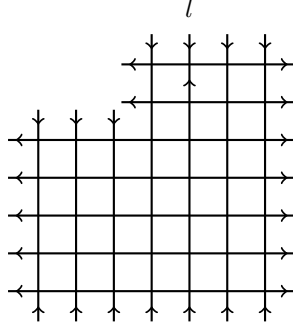


FIGURE 4. Boundary correlation function  $H_{N,r,s}^{(l)}$  in the case  $N = 7$ ,  $r = 4$ ,  $s = 2$ , and  $l = 3$ .

closed form expressions for the partition function and some correlation functions of the model on certain classes of more general domains. For example, the EFP essentially describes the quotient of the partition functions of the model on the L-shaped domain and the original  $N \times N$  lattice, namely, the following relations holds:

$$Z_{N,r,s} = \frac{Z_N}{w_2^{s(N-r)}} G_N^{(r,\dots,r)} = \frac{1}{(1-\alpha)^{s(N-r)/2}} G_N^{(r,\dots,r)}. \quad (2.3)$$

Here the first equality is valid for arbitrary weights while the second is specific for the case of free-fermion weights, with parameterization (2.1), when the partition functions evaluates simply to  $Z_N = 1$ . Thus (2.2), due to (2.3), also provides a multiple integral representation for the partition function.

Below we shall be interested in a particular boundary correlation function for the six-vertex model in an L-shaped domain. To define this function let us consider the first row of vertical edges, between the first two horizontal lines. We note that, as a consequence of the ice-rule and domain wall boundary conditions, the corresponding arrows are all pointing down, except one. We denote by  $H_{N,r,s}^{(l)}$  the probability of observing this sole up arrow exactly on the  $l$ th vertical edge,  $l = 1, \dots, r$ , see Fig. 4. We introduce the corresponding generating function,

$$h_{N,r,s}(w) = \sum_{l=1}^r H_{N,r,s}^{(l)} w^{l-1}, \quad h_{N,r,s}(1) = 1. \quad (2.4)$$

This function plays a crucial role in what follows.

It is clear that the boundary correlation function  $H_{N,r,s}^{(l)}$  is closely connected to the GEFP, upon suitable specialization of the  $r_j$ 's. Indeed, for  $l \leq r$ , the quotient  $G_{N,s}^{(l,r,\dots,r)} / G_{N,s}^{(r,\dots,r)}$  gives the probability of observing, for the model on the L-shaped domain, a left-pointing arrow on the first horizontal edge in the  $l$ th column. The boundary correlation function  $H_{N,r,s}^{(l)}$  is nothing but the lattice derivative in  $l$  of this probability:

$$H_{N,r,s}^{(l)} = \frac{1}{G_{N,s}^{(r,\dots,r)}} \left[ G_{N,s}^{(l,r,\dots,r)} - G_{N,s}^{(l-1,r,\dots,r)} \right], \quad l = 1, \dots, r. \quad (2.5)$$

The generating function  $h_{N,r,s}(w)$  can similarly be expressed in terms of the GEFP, with some simplifications occurring at the level of the integrand in (2.2).

An analogous quantity could be defined for the refinement position on a different boundary side: in the  $(s + 1)$ th row of vertical edges, restricted to the last  $N - r$  columns, there is at most one arrow pointing up (and in fact, in the limit of large  $N$ , almost surely one). In order to investigate the associated statistics, one may study the lattice derivative (in  $l$ ) of the correlation function  $G_{N,s+1}^{(r,\dots,r,l)} / G_{N,s}^{(r,\dots,r)}$ , with  $r \leq l \leq N$ . As in this paper we are considering only the free-fermionic case, in which the exact knowledge of a portion of the curve implies the knowledge of all the curve, by analytic continuation, we can avoid the study of this second combination (although, in fact, at the level of the study of the log-gas, this would require only minor modifications).

**2.3. Scaling limit, Arctic ellipse, and two regimes.** The phase separation phenomena in the six-vertex model take place in the scaling limit, which is performed by sending  $N \rightarrow \infty$ , and simultaneously rescaling the lattice coordinates  $(j, k)$  such that:  $j/N = x$ ,  $k/N = y$ , with  $(x, y) \in [0, 1]^2$  now being continuous coordinates. In the case of the L-shaped domain, the parameters  $r$  and  $s$  are rescaled as well, and we set

$$R = \frac{r}{s}, \quad Q = \frac{N - r - s}{s}, \quad (2.6)$$

where  $R \geq 1$  (in order for the statistical ensemble to be nontrivial) and, without loss of generality,  $Q \geq 0$  (the case  $Q < 0$  may be obtained by symmetry). We use  $s$ , rather than  $N$ , as the main scaling parameter since the former naturally appears in the discrete log-gas description of the model.

The  $R$  and  $Q$  fully describe the geometry of L-shaped region in the scaling limit. An alternate useful parametrization is given by the coordinates of the bottom-right vertex of the rectangular cut-off corner of the L-shaped domain:

$$\xi_x = \frac{R}{R + Q + 1}, \quad \xi_y = \frac{1}{R + Q + 1}. \quad (2.7)$$

Thus, in the scaling limit, the L-shaped domain is rescaled into the region  $\{[0, \xi_x] \times [0, \xi_y]\} \cup \{[0, 1] \times [\xi_y, 1]\}$  of the  $\mathbb{R}^2$  plane, see Fig. 5. Note that the coordinates  $x$  and  $y$  have origin in correspondence of the top-right vertex of the L-shaped domain, and are oriented leftward and downward, respectively. This unconventional choice is done in order to match with the labeling of the rows and columns in the discrete lattice.

It is known [40, 41] that the model undergoes a third-order phase transition as the cut-off rectangle is large enough to touch the Arctic ellipse of the model on the original (unmodified) lattice. More precisely, the phase transition occurs, for given values of  $Q$  and  $\alpha$ , at  $R = R_c(Q, \alpha)$ :

$$R_c = \frac{\left(1 + \sqrt{\alpha(1 + Q)}\right)^2}{1 - \alpha}. \quad (2.8)$$

This curve splits the space of parameters  $(R, Q, \alpha) \in [1, \infty) \times [0, \infty) \times [0, 1]$  into two regions, which we call Regime I, when  $R \in [R_c, \infty)$ , and Regime II,  $R \in [1, R_c]$ .

In terms of the coordinates  $\xi_x$  and  $\xi_y$ , the value  $R_c$  corresponds to one arc of the ellipse

$$\frac{(1 - x - y)^2}{1 - \alpha} + \frac{(x - y)^2}{\alpha} = 1, \quad (2.9)$$

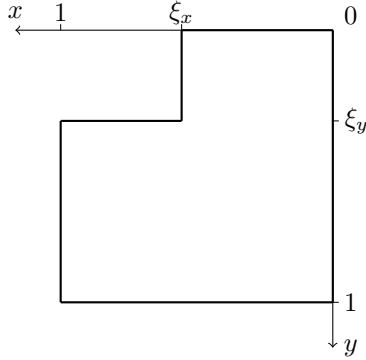


FIGURE 5. The portion of the  $\mathbb{R}^2$  plane corresponding to the L-shaped domain in the scaling limit.

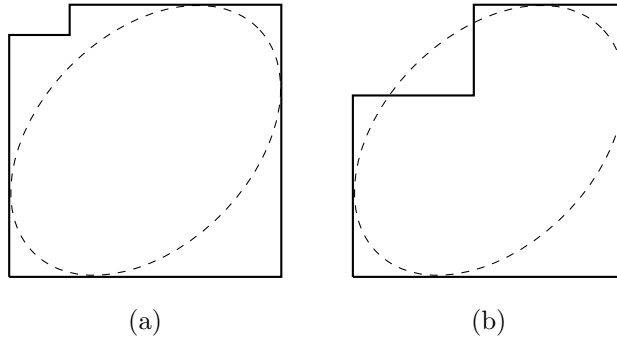


FIGURE 6. The two regimes: (a) Regime I, (b) Regime II.

tangent to the four sides of the unit square, and specifically to that arc which connects tangency points  $(x, y) = (\alpha, 0)$  and  $(x, y) = (1, 1 - \alpha)$ . This arc is also described by the equation  $\sqrt{y} = \sqrt{(1 - \alpha)x} - \sqrt{\alpha(1 - x)}$ .

In other words, (2.9) is nothing but the Arctic ellipse of the original six-vertex model (at the free-fermion point). Then, Regime I corresponds to the situation where the cut-off rectangle lies totally outside the Arctic ellipse; in Regime II the cut-off rectangle ‘penetrates’ the interior of the Arctic ellipse, see Fig. 6. In the former case the arctic curve is not modified by the restricted geometry, while in latter case it must be deformed into some new curve, whose determination is the goal here.

In the case of the L-shaped domain with domain wall boundary conditions, phase separation phenomena and the emergence of a nontrivial limit shape should be expected, on the basis of the general results of [18–20]. On top of this, the phenomenon is clearly observed in numerics, see Fig. 7. The numerics presented in this picture has been generated basing on the generalized domino shuffling algorithm [44], see Appendix A for details.

The analytic determination of the arctic curve of the model is a nontrivial problem. In the free-fermion case, one could in principle resort to the general



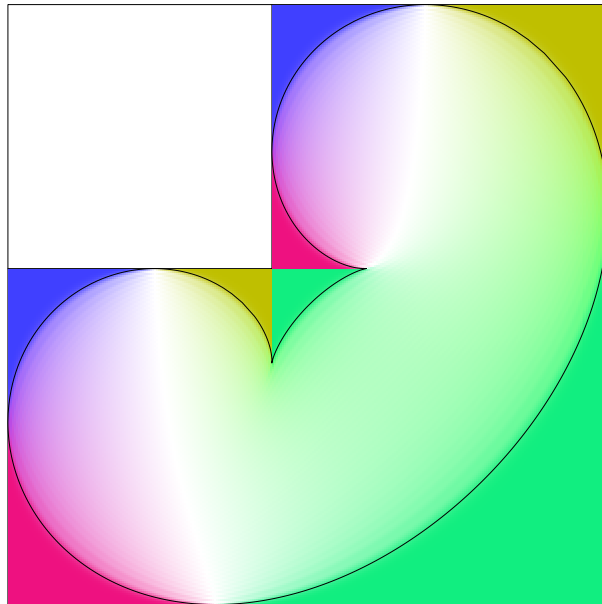


FIGURE 7. Illustration of the edge-inclusion probabilities, in the domain with  $N = 300$  and  $s = N - r = 132$ , done according to the ‘Limit shape’ procedure described in Appendix A. In black, the plot of the arctic curve (4.17) with the same ratios  $r/N$  and  $s/N$ .

approach developed for dimer models in [18–20]. However, for the square lattice, the characteristic polynomial of the corresponding Kasteleyn matrix is of degree higher than one, and makes it difficult to work out explicit results beyond the case of the square domain.

Here we shall resort to the Tangent method, that determines the Arctic curve of the six-vertex model in a generic domain as the geometric caustic of a family of straight lines, that are completely determined by the behaviour of the boundary correlation function in the scaling limit [36]. We emphasize that this paper provides just one application of the general method, which instead applies, in principle, to a wide class of domains and to generic Boltzmann weights.

### 3. The Tangent method

In the section we illustrate how the Tangent method may be applied to the six-vertex model on an L-shaped domain with domain wall boundary conditions. Our main object of study is the one-point boundary correlation function, whose asymptotic behaviour in the scaling limit determines the arctic curve. The boundary correlation function may be represented in terms of a discrete log-gas. Correspondingly, we show that its scaling limit behaviour is described by (the functional inverse of) the resolvent associated to the discrete log-gas in the thermodynamic limit.

**3.1. Parametric equation for the arctic curve.** In the case of the L-shaped domain, the Tangent method gives the following recipe: the arc of the arctic curve subtended by the corner with lattice coordinates  $(r, 1)$ , i.e.,  $(\xi_x, 0)$  in

the scaling limit, can be expressed in parametric form  $x = x(w)$ ,  $y = y(w)$ , with  $w \in [1, \infty)$ , as the solution of the linear system of equations

$$F(w; x, y) = 0, \quad \partial_w F(w; x, y) = 0, \quad (3.1)$$

with

$$F(w; x, y) = x - M(w)y - \Phi(w), \quad M(w) \equiv \frac{w}{(w-1)(\alpha w + 1 - \alpha)}. \quad (3.2)$$

Here the function  $\Phi(w) = \Phi(w; R, Q, \alpha)$  is defined as follows:

$$\Phi(w) = \lim_{N, r, s \rightarrow \infty} \frac{1}{N} w \partial_w \log h_{N, r, s}(w), \quad (3.3)$$

where  $h_{N, r, s}(w)$  is the generating function of the boundary correlation function  $H_{N, r, s}^{(l)}$ , see (2.4).

Note that the recipe may be equivalently formulated as follows: the above considered arc of arctic curve is the geometric caustic of the one-parameter family (3.2) of straight lines in the  $(x, y)$ -plane, in the parameter  $w \in [1, \infty)$ . Also, the values  $w = 1$ , and  $w \rightarrow \infty$  correspond to the two points of contact of the considered arc with the two sides of the L-shaped domain:  $\{(x, 0), x \in [0, \xi_x]\}$  and  $\{(\xi_x, y), y \in [0, \xi_y]\}$ , respectively.

The above recipe follows from the ‘path description’ of the six-vertex model, and can be applied to all those models whose configurations can be rephrased in terms of (directed) non-intersecting lattice paths (although the paths are allowed to ‘osculate’, that is, they may have a contact-point interaction). The path description highlights some conservation law of the models and displays their underlying fermionic (but not necessarily free-fermionic) character.

These paths can also be interpreted as level lines of a certain height function, whose value at the boundary is fixed. This height function, in the scaling limit, may converge to some limit shape. Frozen regions are associated to portions of the limit shape which are flat. In this picture, and under the mild assumption that the typical distance between consecutive paths is  $o(N)$ , it is clear that the limiting behaviour of the outmost path describes (some portion of) the arctic curve. The idea is then to condition one end-point of the most external lattice path to some distant lattice point. In the scaling limit, the path is expected to follow only a portion of the outer shell of path (that is, the arctic curve), then to escape it tangentially, and, free from the influence of other paths (as the paths only interact locally), to continue toward the prescribed end-point along a straight line.

This heuristic picture has an analytic counterpart at the level of the boundary correlation function associated to prescribing the position of the end-point, and modulo the very reasonable and strongly supported, but still unproven, tangency assumption, may be developed rigorously. A standard saddle-point analysis leads to the Tangent method’s recipe. According to the above interpretation, for each value of  $w \in [1, \infty)$ , in the scaling limit, the slope of the straight portion of the out-most path is  $1/M(w)$ , while the quantity  $\Phi(w)$  is essentially the value of concentration in  $l$  for the boundary correlation function  $H_{N, r, s}^{(l)}$ ; that is, in the generating function  $h_{N, r, s}(w)$  (see (2.4)), the most relevant summands are concentrated around  $l = \Phi(w)$ , within a window of the order  $\sqrt{N}$ . For a full description of the Tangent method, with many examples, see [36]. For further applications, see [28, 29].

In principle, the above procedure should be performed for each corner of the domain, to determine the corresponding subtended arc of the arctic curve. However, in the considered case of free-fermion Boltzmann weights, the arctic curve is known to be algebraic [18], allowing for the possibility of extending one arc to a full component of the arctic curve, just by analytic continuation. In our case this accounts to extending the range of parameter  $w$  to the whole real axis, and taking both determinations in a certain square root expression.

Clearly, the implementation of the Tangent method requires the explicit knowledge of  $\Phi(w)$ , and thus the calculation of the boundary correlation function  $H_{N,r,s}^{(l)}$ , and the evaluation of the asymptotic behaviour of the corresponding generating function in the scaling limit. This is our main task below.

**3.2. Discrete log-gas representation.** Different representations, in terms of multiple integrals, or of determinants, can be worked out for  $H_{N,r,s}^{(l)}$ , and for the corresponding generating function,  $h_{N,r,s}(w)$ . The most convenient one for our purposes is in terms of a discrete log-gas:

PROPOSITION 3.1. *For the generating function  $h_{N,r,s}(w)$  the following representation is valid:*

$$h_{N,r,s}(w) = \frac{w^{r-1} I_{N,r,s}(u)}{I_{N,r,s}(1)}. \quad (3.4)$$

Here, the variables  $u$  and  $w$  are related by

$$u = \frac{\alpha w + 1 - \alpha}{w}, \quad (3.5)$$

and the function  $I_{N,r,s}(u)$  is given as

$$I_{N,r,s}(u) = \sum_{m_1, \dots, m_s=0}^{r-1} \prod_{j=1}^s \mu_{N-r-s}^{\alpha}(m_j) \prod_{1 \leq j < k \leq s} (m_k - m_j)^2 \times \oint_{C_{m_1, \dots, m_s}} \frac{\sigma(u, z)}{\prod_{j=1}^s (z - m_j)} \frac{dz}{2\pi i}, \quad (3.6)$$

where

$$\mu_q^{\alpha}(m) = \alpha^m \binom{q+m}{q}, \quad m \in \mathbb{N}_0, \quad (3.7)$$

and

$$\sigma(u, z) = (s-1)! \frac{u^{r+s-z-2}}{(1-u)^{s-1}}. \quad (3.8)$$

The integration in (3.6) is over a simple counterclockwise oriented contour enclosing all  $m_j$ 's, and no other singularity of the integrand.

The proof of proposition 3.1 is provided in appendix B, and it goes along the lines of what is done in [39] in absence of refinement, that is, for the quantity  $I_{N,r,s}(1)$ .

Concerning the statements of Proposition 3.1 several remarks are in order. First, we note that  $w = (1-\alpha)/(u-\alpha)$ , and so  $w \rightarrow 1$  as  $u \rightarrow 1$ , hence (3.4) reproduces the normalization condition  $h_{N,r,s}(1) = 1$ , see (2.4).

Second, even though the function  $\sigma(u, z)$  is singular as  $u \rightarrow 1$ , the integral in (3.6) is regular at  $u = 1$ . Indeed, for any fixed  $s$ , the integral over  $z$  in (3.6) can be estimated as  $u \rightarrow 1$  as follows:

$$\oint_{C_{m_1, \dots, m_s}} \frac{\sigma(u, z)}{\prod_{j=1}^s (z - m_j)} \frac{dz}{2\pi i} = (s-1)! \frac{u^{s+r-2}}{(1-u)^{s-1}} \oint_{C_{m_1, \dots, m_s}} \frac{e^{-z \log u}}{\prod_{j=1}^s (z - m_j)} \frac{dz}{2\pi i} \\ \sim \frac{u^{s+r-2}}{(1-u)^{s-1}} (-\log u)^{s-1} \sim 1. \quad (3.9)$$

Third, the quantity  $I_{N,r,s}(1)$  reads

$$I_{N,r,s}(1) = \sum_{m_1, \dots, m_s=0}^{r-1} \prod_{j=1}^s \mu_{N-r-s}^\alpha(m_j) \prod_{1 \leq j < k \leq s} (m_k - m_j)^2. \quad (3.10)$$

From this expression it follows that  $I_{N,r,s} \equiv I_{N,r,s}(1)$  can be viewed as the partition function of a discrete log-gas confined within a finite interval, note the condition  $0 \leq m_j < r$ ,  $j = 1, \dots, s$ , for the particle coordinates. Correspondingly, the quantity  $I_{N,r,s}(u)$  can be viewed as a particular correlation function of the discrete log-gas defined by (3.10). The discrete weight (3.7) is that of the Meixner polynomials. The partition function and free energy of this log-gas with discrete measure (3.7) have been studied in details in [38], see also [45]. The role and consequences of the condition  $0 \leq m_j < r$ ,  $j = 1, \dots, s$  on the behaviour of the free energy have been discussed in [40, 41].

**3.3. Relation between  $\Phi(w)$  and the resolvent of the log-gas.** To proceed further, we need to evaluate the quantity  $\Phi(w)$  defined in (3.3). Recalling (3.4), we may write

$$\Phi(w) = \frac{1}{R+Q+1} \left( R + w \frac{\partial u}{\partial w} \lim_{N,r,s \rightarrow \infty} \frac{1}{s} \partial_u \log I_{N,r,s}(u) \right), \quad (3.11)$$

and thus we need to estimate the large  $s$  behaviour of the correlation function  $I_{N,r,s}(u)$  for the discrete log-gas with measure (3.7) in a scaling limit with  $r/s$  and  $N/s$  fixed.

Let us focus first on the partition function  $I_{N,r,s}$  of the same discrete log-gas. Its large  $s$  behaviour may be determined in the saddle-point approximation. The standard procedure is to rescale the eigenvalues by a factor  $s$ , namely  $m_j \rightarrow sz_j$ . After rescaling, the sums in (3.10) can be reinterpreted as Riemann sums, and, in the large- $s$  limit, replaced by integrals:

$$I_{N,r,s} \propto \int_0^R \cdots \int_0^R dz_1 \cdots dz_s \prod_{j=1}^s \mu_{N-r-s}^\alpha(\lfloor sz_j \rfloor) \prod_{1 \leq j < k \leq s} (z_k - z_j)^2 \quad (3.12)$$

Now the usual saddle-point analysis for Random Matrix models can be applied, provided that one imposes a suitable additional constraint accounting for the discreteness of the  $m_j$ 's [46], see [40, 41] for full details on the specific example of (3.10). The solution  $\{\tilde{z}_j\}_{j=1, \dots, s}$  of the set of saddle-point equations associated to the multiple integrals in (3.12) is encoded in the resolvent  $W(z)$ , defined as

$$W(z) = \lim_{s \rightarrow \infty} \frac{1}{s} \sum_{j=1}^s \frac{1}{z - \tilde{z}_j}. \quad (3.13)$$

In the case of  $I_{N,s,r}(u)$ , rescaling the log-gas ‘coordinates’  $m_j \rightarrow sz_j$  and simultaneously replacing  $z \rightarrow sz$ , we get

$$I_{N,r,s}(u) \propto \int_0^R \cdots \int_0^R dz_1 \cdots dz_s \prod_{j=1}^s \mu_{N-r-s}^\alpha(\lfloor sz_j \rfloor) \prod_{1 \leq j < k \leq s} (z_k - z_j)^2 \times \oint_{C_{z_1, \dots, z_s}} \frac{\sigma(u, sz)}{\prod_{j=1}^s (z - z_j)} dz, \quad (3.14)$$

The crucial point is that the set of saddle-point equations for the  $z_j$ ’s remains the same as for the case of  $I_{N,r,s}$ , and the corresponding solution is still encoded in  $W(z)$ . However, there is an additional saddle-point equation, relative to the variable  $z$ , which, recalling (3.8), reads

$$-\log u = W(\tilde{z}). \quad (3.15)$$

In other words, the saddle-point value for the extra integration variable is given by the functional inverse of the resolvent:

$$\tilde{z} = W^{-1}(-\log u). \quad (3.16)$$

The inversion relation (3.16) appears in several settings, see, e.g., [47].

Differentiating the logarithm of (3.14) with respect to  $u$ , we find

$$\partial_u \log I_{N,r,s}(u) = \langle \partial_u \log \sigma(u, sz) \rangle \quad (3.17)$$

where brackets  $\langle \cdot \rangle$  denote the expectation value with respect to the measure associated to  $I_{N,r,s}(u)$ , see (3.14). Taking into account that

$$\partial_u \log \sigma(u, sz) = \frac{s}{1-u} + \frac{s+r-sz}{u} \quad (3.18)$$

and using that in the scaling limit  $\langle z \rangle = \tilde{z}$ , we get

$$\lim_{N,r,s \rightarrow \infty} \frac{1}{s} \partial_u \log I_{N,r,s}(u) = \frac{1}{1-u} + \frac{1+R-W^{-1}(-\log u)}{u}, \quad (3.19)$$

where we also have made use of (3.16). Finally, using (3.11) and (3.4), we get

$$\Phi(w) = \frac{1}{(R+Q+1)u} \left[ R\alpha + \frac{u-\alpha}{u-1} + (u-\alpha)W^{-1}(-\log u) \right], \quad (3.20)$$

where variables  $u$  and  $w$  are related by (3.5).

Thus, the evaluation of  $\Phi(w)$  has boiled down to that of (the functional inverse of)  $W(z)$ , that is the resolvent associated to the discrete log-gas (3.10). The expressions of this resolvent for the various regimes has been worked out in [40, 41].

#### 4. Equation for the arctic curve

In this section we focus on details of derivation of the arctic curve using the results of Ref. [41] on the explicit form of the resolvent  $W(z)$ . We consider various cases, in order of increasing complexity: we start with Regime I, next we consider Regime II for a symmetric domain (the cut-off rectangle is a square) that corresponds to  $Q = 0$ , and, finally, we treat the case of Regime II in full generality ( $Q \geq 0$ ).

**4.1. Regime I.** In this case,  $R > R_c$ , and  $R$  does not enter the expression of the resolvent, which reads (see [40]):

$$W(z) = -\log \sqrt{\alpha} - \log \frac{\sqrt{a(z-b)} + \sqrt{b(z-a)}}{\sqrt{(b-a)z}} \mp \log \frac{\sqrt{(a+Q)(z-b)} + \sqrt{(b+Q)(z-a)}}{\sqrt{(b-a)z}}, \quad (4.1)$$

where

$$a = \frac{\left(1 - \sqrt{\alpha(1+Q)}\right)^2}{1-\alpha}, \quad b = \frac{\left(1 + \sqrt{\alpha(1+Q)}\right)^2}{1-\alpha}. \quad (4.2)$$

In (4.1) the choice of the sign depends on the value of the parameter  $Q$ , with the critical value  $Q_c = \alpha^{-1} - 1$  corresponding to the case where  $a = 0$ ; the minus sign corresponds to  $Q < Q_c$  and the plus sign to  $Q > Q_c$ . Solving equation  $-\log u = W(z)$  for  $z$ , we get the following solution valid in both cases:

$$z = -\frac{[1 - \alpha(1+Q)]u + \alpha Q}{(u-1)(u-\alpha)}, \quad Q \in [0, \infty). \quad (4.3)$$

The function (3.20) reads

$$\Phi(w) = \frac{\alpha}{u} = \frac{\alpha w}{\alpha w + 1 - \alpha}. \quad (4.4)$$

Note that dependence from  $Q$  and  $R$  cancel out in the expression of  $\Phi(w)$ . Plugging the result into (3.2) and solving of the linear system (3.1) yields

$$x = \frac{\alpha w^2}{\alpha w^2 + 1 - \alpha}, \quad y = \frac{\alpha(1-\alpha)(w-1)^2}{\alpha w^2 + 1 - \alpha}. \quad (4.5)$$

Here, according to the recipe prescribed in Section 3.1 the parameter  $w$  should run over the interval  $[1, \infty)$ . Actually, the rectangular portion removed from the top-left corner to build the L-shaped domain constitutes a forbidden region for the family of lines (3.2). As a result, the parameter  $w$  is, by construction, allowed to run only over the interval  $[1, w_0)$ , where  $w_0$  is the largest of the two solutions of:

$$(w-1)(\alpha w + 1 - \alpha)\xi_x - w\xi_y - \alpha w(w-1) = 0. \quad (4.6)$$

Condition (4.6) selects, within the family of lines (3.2), with  $\Phi(w)$  given by (4.4), the two lines passing through the point of coordinates  $(\xi_x, \xi_y)$ .

Apart from this technical detail, the already mentioned fact that in the presently considered free-fermion case the arctic curve is guaranteed to be algebraic [18] allows anyway to extend the range of  $w$  to the whole real axis,  $w \in \mathbb{R}$ , and correspondingly to describe the whole arctic curve. Indeed, eliminating  $w$  in (4.5) yields the Arctic ellipse (2.9), as expected for the Regime I.

The implicit form of equation of the arctic curve, given by (2.9) can also be directly recovered by considering the polynomial  $P(u) = u(u-1)F(w)$ , where  $F(w) = F(w; x, y)$  is the function defined in (3.2). Explicitly,  $P(u)$  reads

$$P(u) = u(u-1)x + (u-\alpha)y - \alpha(u-1). \quad (4.7)$$

Since system (3.1) implements the condition that two zeroes of the function  $F(w)$  should coincide, we can directly impose this condition by requiring that the discriminant of  $P(u)$  vanish. This immediately gives (2.9).

**4.2. Regime II, symmetric domain.** In Regime II the resolvent  $W(z)$  has in general a rather complicate expression, and it is convenient to focus first on the case of a symmetric domain, where the cut-off rectangle is actually a square. In this case  $s = N - r$ , that is  $Q = 0$ . The Regime II means that the other geometric parameter  $R$  is in the range

$$R : 1 \leq R < R_c, \quad R_c = \frac{1 + \sqrt{\alpha}}{1 - \sqrt{\alpha}}. \quad (4.8)$$

The resolvent reads (see [40]):

$$W(z) = -\log \sqrt{\alpha} + \log \frac{z}{z - R} - 2 \log \frac{\sqrt{a(z-b)} + \sqrt{b(z-a)}}{\sqrt{(R-a)(z-b)} + \sqrt{(R-b)(z-a)}}, \quad (4.9)$$

where

$$a = \frac{(\sqrt{R+1} - \sqrt{(R-1)\sqrt{\alpha}})^2}{2(1 + \sqrt{\alpha})}, \quad b = \frac{(\sqrt{R+1} + \sqrt{(R-1)\sqrt{\alpha}})^2}{2(1 + \sqrt{\alpha})}. \quad (4.10)$$

The relation  $-\log u = W(z)$  can be written in the form:

$$u = \sqrt{\alpha} \frac{(\sqrt{(R-a)(z-b)} - \sqrt{(R-b)(z-a)})(\sqrt{b(z-a)} + \sqrt{a(z-b)})}{(\sqrt{(R-a)(z-b)} + \sqrt{(R-b)(z-a)})(\sqrt{b(z-a)} - \sqrt{a(z-b)})}. \quad (4.11)$$

Using (4.10) and taking into account (4.8), one can simplify it to

$$u = \sqrt{\alpha} \frac{(1 + \sqrt{\alpha})(\sqrt{(z-a)(z-b)} - \sqrt{ab}) + (1 - \sqrt{\alpha})z}{(1 + \sqrt{\alpha})(\sqrt{(z-a)(z-b)} + \sqrt{ab}) - (1 - \sqrt{\alpha})z} \quad (4.12)$$

Solving for  $z$ , we get two solutions:

$$z = \frac{R}{2} - \frac{(1 - \alpha)u}{2(u - \alpha)(u - 1)} \pm \frac{(u - \sqrt{\alpha})\sqrt{R^2(u - \alpha)(u - 1) + (1 + \sqrt{\alpha})^2 u}}{2(u - \alpha)(u - 1)}. \quad (4.13)$$

Apparently, these solutions represent two branches of the same function  $W^{-1}(-\log u)$ , which determines the arctic curve; a particular choice of the sign in (4.13) corresponds to a portion of the arctic curve, via the function (see (3.20))

$$\Phi(w) = \frac{1}{(R+1)u} \left[ R\alpha + \frac{u - \alpha}{u - 1} + (u - \alpha)z \right], \quad (4.14)$$

which reads

$$\Phi(w) = \frac{\alpha}{2u} + \frac{\xi_x}{2} + \frac{\xi_y(u - \alpha)}{2u(u - 1)} \pm \frac{(u - \sqrt{\alpha})\sqrt{\xi_x^2(u - \alpha)(u - 1) + \xi_y^2(1 + \sqrt{\alpha})^2 u}}{2u(u - 1)}. \quad (4.15)$$

Here, we have employed the notations for the coordinates of the bottom-right vertex of the cut-off rectangle,  $\xi_x = R/(R+1)$ ,  $\xi_y = 1/(R+1)$ , see (2.7), and we also recall that the variables  $u$  and  $w$  are related by (3.5).

To investigate the resulting arctic curve, let us denote by  $\Phi_+(w)$  and  $\Phi_-(w)$  the function in (4.15) taken with the plus and minus signs, respectively. Consider two different parametric families of straight lines:

$$F_{\pm}(w) = x - M(w)y - \Phi_{\pm}(w). \quad (4.16)$$

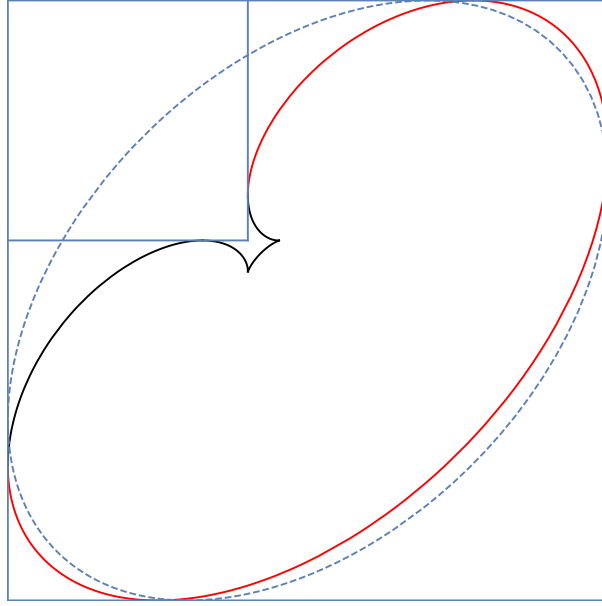


FIGURE 8. Plot of the two components  $\mathcal{C}_-$  and  $\mathcal{C}_+$ , in red (grey in b/w printing) and black, respectively, as given in (4.17); here  $\alpha = 0.3$  (corresponding to  $R_c \simeq 3.42$ ), and  $R = 1.5$ . The dashed line shows, for comparison, the Arctic ellipse (2.9).

Solving the corresponding system of equations (3.1) in  $x$  and  $y$ , we obtain

$$\begin{aligned} x_{\pm}(w) &= -\frac{M(w)\Phi'_{\pm}(w)}{M'(w)} + \Phi_{\pm}(w), \\ y_{\pm}(w) &= -\frac{\Phi'_{\pm}(w)}{M'(w)}, \end{aligned} \tag{4.17}$$

where the prime denotes differentiation with respect to  $w$ . This is the parametric form of the two branches  $\mathcal{C}_+$  and  $\mathcal{C}_-$  of the arctic curve, given respectively by  $(x_+(w), y_+(w))$  and  $(x_-(w), y_-(w))$ , with  $w \in \mathbb{R}$ . These expressions make it possible to produce plots of the arctic curve; Fig. 8 shows an example for particular values of the parameters. In Fig. 9, another example of the curve, corresponding to a different choice of parameters is plotted against numerics. See Appendix A for further details.

The obtained arctic curve has six points of contact with the boundary of the L-shaped domain, and two cusps, for a total of eight special points. Starting from the bottom side of the boundary, and proceeding counterclockwise, the first four points correspond to the values  $w = -(1-\alpha)/\alpha, 0, 1, \infty$ , in  $(x_+(w), y_+(w))$ , while the next four correspond to the same values of  $w$ , in  $(x_-(w), y_-(w))$ . It is apparent from inspection of formula (3.2) that these values of  $w$  indeed correspond to (alternately in cyclic order) vanishing or diverging values for the slope of the arctic curve.

The equation of the arctic curve can also be obtained in an implicit form. Because of the geometry of the curve, it is convenient to introduce *diagonal* coordinates

$$z_1 = x - y, \quad z_2 = 1 - x - y. \tag{4.18}$$



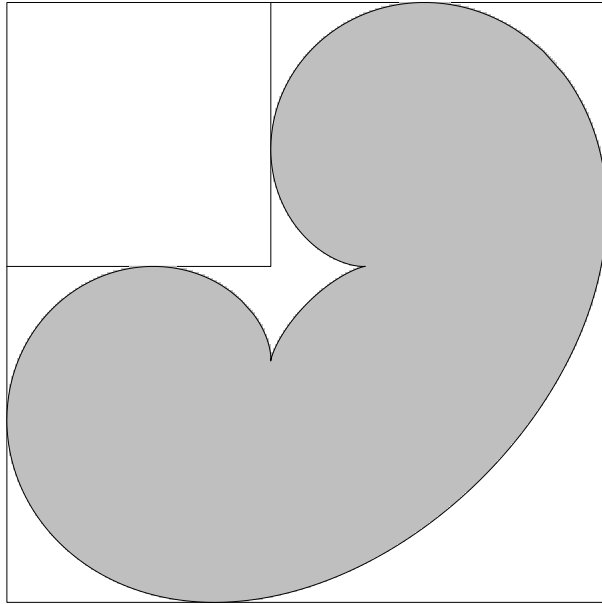


FIGURE 9. In grey, numerical determination of the arctic curve, in the domain with  $N = 300$  and  $s = N - r = 132$ , done according to the ‘Arctic Curve’ procedure described in Appendix A. In black, the plot of the arctic curve (4.17) with the same ratios  $r/N$  and  $s/N$ .

Introduce the functions (we use here the variable  $u$  in the argument):

$$\tilde{F}_{\pm}(u) \equiv 2u(u-1)F_{\pm}(w(u)). \quad (4.19)$$

Explicitly, these functions read

$$\begin{aligned} \tilde{F}_{\pm}(u) = & (z_1 - z_2 - \xi_x)u(u-1) - (z_1 + z_2 + \xi_y)(u-\alpha) + (u-\alpha)u \\ & \pm (u - \sqrt{\alpha})\sqrt{\xi_x^2(u-\alpha)(u-1) + \xi_y^2(1+\sqrt{\alpha})^2u}. \end{aligned} \quad (4.20)$$

Consider the following polynomial of degree 4 in  $u$ :

$$P(u) = \tilde{F}_+(u)\tilde{F}_-(u). \quad (4.21)$$

Clearly, the equation for the arctic curve can be derived by requiring that this polynomial has vanishing discriminant. More precisely, denoting by  $D(P)$  the discriminant of  $P(u)$ , it is fairly easy to see from the formulas above, that  $D(P)$  is a polynomial of degree 8 in  $z_1, z_2$ . Moreover, one can easily verify (using a symbolic manipulation software) that it has the following structure:

$$D(P) = \left( z_1 - \frac{1 + \sqrt{\alpha}}{2} + \xi_y \right)^2 \mathcal{A}(z_1, z_2), \quad (4.22)$$

where  $\mathcal{A}(z_1, z_2)$  is a polynomial of degree 6 in  $z_1$  and  $z_2$ . The equation  $\mathcal{A}(z_1, z_2) = 0$  is the desired implicit equation of the arctic curve.

The straight line of equation described by the first factor in (4.22) is precisely that sole line which is tangent to the arctic curve at two distinct points. Indeed,

let  $w_0 \in [1, \infty)$  be the (unique) solution to the condition  $M(w_0) = 1$ , we have

$$w_0 = \frac{2R_c}{R_c - 1}, \quad \Phi_{\pm}(w_0) = \frac{RR_c - 1}{(R+1)(R_c+1)} = \frac{1 + \sqrt{\alpha}}{2} - \xi_y. \quad (4.23)$$

This component arises as a side effect of the Tangent method.

The explicit expression for  $\mathcal{A}(z_1, z_2)$  which is of degree 6 in  $z_1$  and  $z_2$  is rather lengthy and reported in appendix C (some of its 28 coefficients appear to be zero, but most of them are complicate polynomials in  $R, \alpha$ ). At  $R = 1$ , corresponding to  $\xi_x = \xi_y = 1/2$ , that is to a cut-off square of side  $1/2$ , the equation  $\mathcal{A}(z_1, z_2) = 0$  factorizes into two Arctic ellipses and two coinciding straight lines, tangent to both of them, as expected.

**4.3. Regime II, generic domain.** We now turn to the case  $Q > 0$ , where the cut-off portion is a rectangle rather than a square. In this case, in Regime II, the resolvent reads

$$\begin{aligned} W(z) = & -\log \sqrt{\alpha} + 2 \frac{\log \sqrt{(R-a)(z-b)} + \sqrt{(R-b)(z-a)}}{\sqrt{(b-a)(z-R)}} \\ & - \log \frac{\sqrt{(a+Q)(z-b)} + \sqrt{(a+Q)(z-a)}}{\sqrt{(b-a)z}} \\ & \mp \log \frac{\sqrt{a(z-b)} + \sqrt{a(z-a)}}{\sqrt{(b-a)z}}, \end{aligned} \quad (4.24)$$

where the parameters  $a$  and  $b$ ,  $0 \leq a < b \leq R$ , are to be found from the equations<sup>1</sup>:

$$\begin{aligned} \sqrt{\alpha} \frac{\sqrt{R-a} - \sqrt{R-b}}{\sqrt{R-a} + \sqrt{R-b}} \frac{\sqrt{b} \pm \sqrt{a}}{\sqrt{b+Q} - \sqrt{a+Q}} &= 1, \\ \frac{\pm \sqrt{ab} + \sqrt{(a+Q)(b+Q)} - Q}{2} + \sqrt{(R-a)(R-b)} &= 1. \end{aligned} \quad (4.25)$$

Here, the  $\pm$  signs correspond to what is called in Ref. [41] the Regime IIA,  $Q \leq Q_c$ , and Regime IIB,  $Q > Q_c$ , respectively, where the value  $Q = Q_c$  is determined by the condition  $a = 0$ . In contrast to the  $Q = 0$  case, explicit expressions for  $a$  and  $b$  at  $Q \neq 0$  are cumbersome functions of  $R, Q$  and  $\alpha$ , and in the most compact form they can be written as

$$a = A_+ + A_- - 2\sqrt{A_+A_-}, \quad b = A_+ + A_- + 2\sqrt{A_+A_-}. \quad (4.26)$$

where

$$\begin{aligned} A_+ &= (R+Q+1) \frac{(1+\eta)(1+R\eta)[1+(R+Q)\eta]}{[2+Q+(2R+Q)\eta]^2}, \\ A_- &= (R-1) \frac{(1-\eta)(1+Q+R\eta)[1+Q+(R+Q)\eta]}{[2+Q+(2R+Q)\eta]^2}. \end{aligned} \quad (4.27)$$

and the parameter  $\eta \in [0, 1]$  is a suitable root of the (quartic) equation

$$\alpha \frac{(1+\eta)^2(1+Q+R\eta)[1+(R+Q)\eta]}{(1-\eta)^2(1+R\eta)[1+Q+(R+Q)\eta]} = 1. \quad (4.28)$$

---

<sup>1</sup>In [41] there is a misprint in (2.20), (2.22) and (3.8): In the first factor of the first equation the replacement  $a \leftrightarrow b$  should be made.

For the values of the parameters  $R$ ,  $Q$  and  $\alpha$  belonging to the Regime II (i.e., for  $R < R_c$ , where  $R_c = R_c(Q, \alpha)$  is given by (2.8)) such a root always exists and it is unique [41].

The equation  $-\log u = W(z)$  reads

$$u = \sqrt{\alpha} \frac{\sqrt{(R-a)(z-b)} - \sqrt{(R-b)(z-a)}}{\sqrt{(R-a)(z-b)} + \sqrt{(R-b)(z-a)}} \times \frac{\sqrt{(b+Q)(z-a)} + \sqrt{(a+Q)(z-b)}}{\sqrt{b(z-a)} \mp \sqrt{a(z-b)}}, \quad (4.29)$$

that is

$$\frac{u}{\sqrt{\alpha}} = \frac{K_2 \sqrt{(z-a)(z-b)} + K_1 z + K_0}{L_2 \sqrt{(z-a)(z-b)} + L_1 z + L_0}, \quad (4.30)$$

where

$$\begin{aligned} K_2 &= \sqrt{(R-a)(b+Q)} - \sqrt{(R-b)(a+Q)}, \\ K_1 &= \sqrt{(R-a)(a+Q)} - \sqrt{(R-b)(b+Q)}, \\ K_0 &= a\sqrt{(R-b)(b+Q)} - b\sqrt{(R-a)(a+Q)}, \\ L_2 &= \sqrt{(R-a)b} \mp \sqrt{(R-b)a}, \\ L_1 &= \sqrt{(R-b)b} \mp \sqrt{(R-a)a}, \\ L_0 &= \pm b\sqrt{(R-a)a} - a\sqrt{(R-b)b}. \end{aligned} \quad (4.31)$$

Solving (4.30) for  $z$ , we get

$$z = \frac{M_0 M_1 + \left(\frac{a+b}{2}\right) M_2^2 \pm M_2 \sqrt{(aM_1 + M_0)(bM_1 + M_0) + \left(\frac{b-a}{2}\right)^2 M_2^2}}{M_2^2 - M_1^2}, \quad (4.32)$$

where  $M_i = M_i(u)$  are linear functions of  $u$ :

$$M_i = L_i \frac{u}{\sqrt{\alpha}} - K_i, \quad i = 0, 1, 2. \quad (4.33)$$

Using the first equation in (4.25), it can be shown that

$$M_2^2 - M_1^2 = \frac{(b-a)^2}{\alpha} (u - \alpha)(u - 1). \quad (4.34)$$

Hence, for the function  $\Phi(w)$  defined by (3.20), we obtain the following expression:

$$\begin{aligned} \Phi(w) &= \frac{1}{(R+Q+1)u(u-1)} \left\{ (R\alpha+1)u - \alpha(R+1) + \alpha \frac{M_0 M_1 + \left(\frac{a+b}{2}\right) M_2^2}{(b-a)^2} \right. \\ &\quad \left. \pm \frac{\sqrt{\alpha} M_2}{2(b-a)} \sqrt{\frac{4\alpha(aM_1 + M_0)(bM_1 + M_0)}{(b-a)^2} + \alpha M_2^2} \right\}. \end{aligned} \quad (4.35)$$

Here, some terms can be simplified; for example, using just (4.31), one may find that

$$\alpha \frac{M_0 M_1 + \left(\frac{a+b}{2}\right) M_2^2}{(b-a)^2} = Ru^2 + c_1 u + \alpha(R-Q), \quad (4.36)$$

where, however, the coefficient of the linear term,  $c_1$ , in contrast to other coefficients possesses a rather bulky expression even when (4.26) is invoked. The same can be

inferred about the coefficients of the quadratic polynomial in  $u$  standing under the square root sign in (4.35).

Nevertheless, the expression (4.35) describes the arctic curve for a generic L-shaped domain. All considerations made above in the  $Q = 0$  case extends to the present case ( $Q \geq 0$ ) as well, concerning both parametric and implicit form of the curve.

Namely, denote  $\Phi_+(w)$  and  $\Phi_-(w)$  the function in (4.35) taken with the plus and minus signs, respectively, and consider two different parametric families of straight lines described by (4.16). Then (4.17) provides a parametric form of two branches of the whole arctic curve. In producing plots of the Arctic curve, the only difference with the  $Q = 0$  case is that now one has first to obtain values of the parameters  $a$  and  $b$  from (4.26), by solving equation (4.28) for at a given set of the main parameters  $R$ ,  $Q$ , and  $\alpha$ , and next to plug all the values into (4.31), which determine the linear functions  $M_i = M_i(u)$  defined by (4.33).

Lastly, one can also address the problem of finding an equation which describes the arctic curve in implicit (rather than in parametric) form. Here, again this equation can be found from the condition of vanishing of the discriminant of the corresponding quartic polynomial  $P(u)$ , constructed from the functions  $F_{\pm}(w)$  by (4.20) and (4.21). The discriminant  $D(P)$ , similarly to (4.22), factors into two straight lines and the arctic curve  $\mathcal{A}(z_1, z_2)$ , which is of degree 6.

## 5. Acknowledgements

We are grateful to A. Abanov, S. Chhita and F. Franchini for interesting discussions. We are indebted to B. Wieland for sharing with us the code for generating uniformly sampled alternating-sign matrices. We thank the Simons Center for Geometry and Physics (SCGP, Stony Brook), research program on ‘Statistical Mechanics and Combinatorics’ and the Galileo Galilei Institute for Theoretical Physics (GGI, Florence), research programs on ‘Statistical Mechanics, Integrability and Combinatorics’ and ‘Entanglement in Quantum Systems’, for hospitality and support at some stage of this work. FC is grateful to LIPN, *équipe* Calin at Université Paris 13, for hospitality and support at some stage of this work. AGP and AS are grateful to INFN, Sezione di Firenze for hospitality and support at some stage of this work. AGP acknowledges partial support from the Russian Science Foundation, grant #18-11-00297.

## Appendix A. Comparison with finite-size results

In this paper we have determined the arctic curve of a free-fermionic model. As a result of the simplifications occurring in this case, with respect to what it would be for a generic six-vertex model prediction, it is much easier to perform a comparison of the result with informations obtained by alternative methods.

In particular, through the correspondence with a model of dimer coverings on a bipartite planar graph, at finite size, a suitable 1-point function in the bulk can be calculated, either from the inverse Kasteleyn matrix, or, more efficiently, through a method, devised by Propp, as part of the Urban Renewal, or Generalised Domino Shuffling, algorithm for the exact sampling of configurations (see [44], Section 3).

Our geometry is particularly adapted to the use of Propp’s algorithm. With respect to the graphical notation in [44] (see in particular Section 1.2), we shall just initialise the weights as in a graph of the form shown in Fig. 10. Then, from the

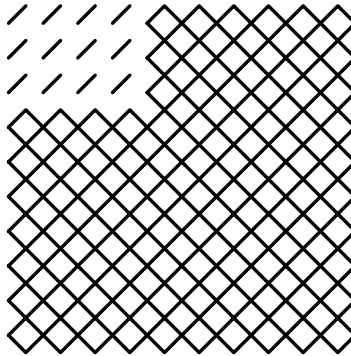


FIGURE 10. The Aztec Diamond graph related to the L-shaped domain.

algorithm we obtain the *edge-inclusion probabilities*, that is, the probabilities  $p_{ij}$ ,  $q_{ij}$ ,  $r_{ij}$  and  $s_{ij}$  that the edges in the plaquette of coordinates  $(i, j)$ , and position NW, NE, SW and SE, respectively, are occupied in an uniformly chosen perfect matching compatible with the domain shape (again notations are chosen as to match with those in [44]). Frozen regions correspond to coordinates  $(i, j)$  such that the quadruples  $(p_{ij}, q_{ij}, r_{ij}, s_{ij})$  are equal to  $(1, 0, 0, 0)$ ,  $(0, 1, 0, 0)$ , etc., up to corrections exponentially small in the size of the domain. We represent graphically these four functions in a compact way, with two different strategies, aiming at representing the arctic curve, or, instead, the limit shape.

In the first case, consider the combination

$$x_{ij} = \frac{1}{2}(1 + p_{ij} - q_{ij} - r_{ij} + s_{ij}), \quad (\text{A.1})$$

associated to each plaquette, that is valued in  $[0, 1]$ , and is near to 0 or to 1 in the frozen regions (it is the local fraction of dimers which are oriented diagonally, instead that anti-diagonally). We plot in gray the plaquettes  $(i, j)$  such that  $x_{ij}$  is valued in  $[\varepsilon, 1 - \varepsilon]$ , where  $\varepsilon = N^{-2/3}$ . The scaling of this threshold marks the change of regime between typical and atypical local fluctuations of the arctic curve [38]. The choice of the multiplicative constant 1 is of no special significance, and any other finite constant would have produced similar results. The comparison with our analytic prediction, shown in Figure 9, is remarkably good (everywhere within one lattice spacing).

In the second case, a more refined visualization of the edge-inclusion probabilities is obtained by associating to a plaquette the complex number

$$z_{ij} = \sqrt{p_{ij}} + i\sqrt{q_{ij}} - i\sqrt{r_{ij}} - \sqrt{s_{ij}}. \quad (\text{A.2})$$

This quantity is valued in the disk of radius 1, and is exponentially near to 1,  $i$ ,  $-1$  or  $-i$ , if the plaquette is in a frozen region. We make a coloured plot of the domain, with hue determined according to the argument of  $z_{ij}$ , and brightness determined according to the absolute value of  $z_{ij}$  (so that the colour is near to white in the liquid region). The data are shown in Figure 7.

### Appendix B. Proof of Proposition 3.1

We present here the derivation of representation (3.4) for the generating function  $h_{N,r,s}(w)$ , which is defined by (2.4) and (2.5). It can be written as

$$h_{N,r,s}(w) = \frac{F_{N,r,s}(w)}{F_{N,r,s}(1)}, \quad (\text{B.1})$$

where

$$F_{N,r,s}(w) = \sum_{r_1=1}^r \left( G_{N,s}^{(r_1,r,\dots,r)} - G_{N,s}^{(r_1-1,r,\dots,r)} \right) w^{r_1-1}. \quad (\text{B.2})$$

Note that  $F_{N,r,s}(1) = G_{N,s}^{(r,\dots,r)}$  is the EFP of the six-vertex model with domain wall boundary conditions ( $F_{N,r,s}(1) \equiv F_N^{(r,s)}$ , in the notation of [37]). Change of the integration variables  $z_j \mapsto x_j = (\alpha z_j + 1 - \alpha)/z_j$ ,  $j = 1, \dots, s$ , in (2.2) yields

$$\begin{aligned} G_{N,s}^{(r_1,\dots,r_s)} &= (-1)^{\frac{s(s-1)}{2}} \prod_{j=1}^s (1-\alpha)^{N-r_j} \\ &\times \oint_{C_\infty} \cdots \oint_{C_\infty} \prod_{j=1}^s \frac{x_j^{N-j}}{(x_j - \alpha)^{N-r_j} (x_j - 1)^{s-j+1}} \prod_{1 \leq j < k \leq s} (x_k - x_j) \frac{d^s x}{(2\pi i)^s}, \end{aligned} \quad (\text{B.3})$$

where  $C_\infty$  denotes a circular contour of large radius around the origin (thus enclosing the points  $x = \alpha$  and  $x = 1$ ). Hence,

$$\begin{aligned} F_{N,r,s}(w) &= (-1)^{\frac{s(s-1)}{2}} (1-\alpha)^{(N-r)s} w^{r-1} \\ &\times \oint_{C_\infty} \cdots \oint_{C_\infty} \frac{x_1^{N-1}}{(x_1 - \alpha)^{N-r} (x_1 - 1)^{s-1} (x_1 - u)} \\ &\times \prod_{j=2}^s \frac{x_j^{N-j}}{(x_j - \alpha)^{N-r} (x_j - 1)^{s-j+1}} \prod_{1 \leq j < k \leq s} (x_k - x_j) \frac{d^s x}{(2\pi i)^s}, \end{aligned} \quad (\text{B.4})$$

where  $u = (\alpha w + 1 - \alpha)/w$ . Using

$$\det [(x_{s-k+1} - \alpha)^{s-j}]_{j,k=1,\dots,s} = \prod_{1 \leq j < k \leq s} (x_k - x_j) \quad (\text{B.5})$$

we can write  $F_{N,r,s}(w)$  in the form of an  $s \times s$  determinant

$$F_{N,r,s}(w) = (-1)^{\frac{s(s-1)}{2}} (1-\alpha)^{s(s+q)} w^{r-1} \det A(u), \quad (\text{B.6})$$

where the matrix  $A(u)$  contains dependence on  $u$  only in the last column

$$A_{jk}(u) = \begin{cases} \oint_{C_\infty} \frac{x^{r+q+k-1}}{(x-\alpha)^{q+j} (x-1)^k} \frac{dx}{2\pi i} & k \neq s \\ \oint_{C_\infty} \frac{x^{r+q+s-1}}{(x-\alpha)^{q+j} (x-1)^{s-1} (x-u)} \frac{dx}{2\pi i} & k = s, \end{cases} \quad (\text{B.7})$$

and where we have set  $N = r + s + q$ ,  $q \geq 0$ .

To proceed with (B.6), it is useful to consider first the case  $w = 1$ , that corresponds to  $u = 1$ . Using

$$\begin{aligned} \oint_{C_\infty} \frac{x^c}{(x-\alpha)^a(x-\beta)^b} \frac{dx}{2\pi i} &= \frac{1}{(a-1)!(b-1)!} \partial_\alpha^{a-1} \partial_\beta^{b-1} \oint_{C_\infty} \frac{x^c}{(x-\alpha)(x-\beta)} \frac{dx}{2\pi i} \\ &= \sum_{m=a-1}^{c-b} \binom{m}{a-1} \binom{c-m-1}{b-1} \alpha^{m-a+1} \beta^{c-m-b}, \quad a, b, c \in \mathbb{N}, \end{aligned} \quad (\text{B.8})$$

for the entries of the matrix  $A \equiv A(1)$ , upon setting  $\beta = 1$ ,  $a = q + j$ ,  $b = k$ , and  $c = r + q + k - 1$  and making the change  $m \mapsto m + q$ , we get

$$A_{jk} = \sum_{m=j-1}^{r-1} \binom{m+q}{q+j-1} \binom{r+k-2-m}{k-1} \alpha^{m-j+1}. \quad (\text{B.9})$$

Consider now entries of a given column; since

$$\binom{m+q}{q+j-1} = \frac{q!}{(q+j-1)!} \binom{m+q}{q} (m)_{j-1}, \quad (\text{B.10})$$

where  $(m)_a := m(m-1)\dots(m-a+1)$  denotes the falling factorial, we have

$$A_{jk} = \frac{q!}{(q+j-1)! \alpha^{j-1}} \tilde{A}_{jk} \quad (\text{B.11})$$

where

$$\tilde{A}_{jk} = \sum_{m=0}^{r-1} \binom{m+q}{q} (m)_{j-1} \binom{r+k-2-m}{k-1} \alpha^m, \quad (\text{B.12})$$

and hence

$$\det A = \frac{(q!)^s}{\prod_{j=0}^{s-1} (q+j)!} \alpha^{-\frac{s(s-1)}{2}} \det \tilde{A}. \quad (\text{B.13})$$

The determinant of  $\tilde{A}$  evaluates as follows

$$\begin{aligned} \det \tilde{A} &= \sum_{m_1, \dots, m_s=0}^{r-1} \prod_{k=1}^s \binom{m_k+q}{q} \binom{r+k-2-m_k}{k-1} \prod_{l < k} (m_k - m_l) \alpha^{m_1 + \dots + m_s} \\ &= \frac{(-1)^{\frac{s(s-1)}{2}}}{\prod_{j=0}^s j!} \sum_{m_1, \dots, m_s=0}^{r-1} \prod_{k=1}^s \binom{m_k+q}{q} \prod_{l < k} (m_k - m_l)^2 \alpha^{m_1 + \dots + m_s}, \end{aligned} \quad (\text{B.14})$$

where we have used the fact that  $(m)_{j-1}$  is a monic polynomial of degree  $j-1$  in  $m$ , and, similarly, that  $\binom{r+k-2-m}{k-1}$  is a polynomial of degree  $k-1$  in  $m$ , with the leading coefficient  $(-1)^{k-1}/(k-1)!$ . In total, our calculation amounts to

$$\begin{aligned} F_{N,r,s}(1) &= \frac{(q!)^s}{\prod_{j=0}^{s-1} (q+j)! \prod_{j=0}^s j!} \frac{(1-\alpha)^{s(s+q)}}{\alpha^{\frac{s(s-1)}{2}}} \\ &\quad \times \sum_{m_1, \dots, m_s=0}^{r-1} \prod_{j=1}^s \binom{m_j+q}{q} \prod_{l < k} (m_k - m_l)^2 \alpha^{m_1 + \dots + m_s}. \end{aligned} \quad (\text{B.15})$$

Note that this representation may equivalently be written as

$$F_{N,r,s}(1) = \frac{(q!)^s}{\prod_{j=0}^{s-1} (q+j)! j!} \frac{(1-\alpha)^{s(s+q)}}{\alpha^{\frac{s(s-1)}{2}}} \det \left[ \sum_{m=0}^{r-1} \binom{m+q}{q} m^{j+k-2} \alpha^m \right]_{j,k=1,\dots,s}, \quad (\text{B.16})$$

in agreement with [38, 39].

Consider now the case of generic  $w$ . To apply the derivation above with a minimal modification, consider instead of the matrix  $A(u)$  some matrix  $B(u)$ , which differs from  $A(u)$  only in the entries of the last column,

$$B_{js}(u) = \oint_{\mathcal{C}_\infty} \frac{x^{r+q}}{(x-\alpha)^{q+j}} \left( \frac{x^{s-1}}{(x-1)^{s-1}(x-u)} + \sum_{k=1}^{s-1} \gamma_k \frac{x^{k-1}}{(x-1)^k} \right) \frac{dx}{2\pi i}, \quad (\text{B.17})$$

where  $\gamma_k$ ,  $k=1, \dots, s-1$ , are some constants in  $x$ . Note that  $\det A(u) = \det B(u)$ . For  $\gamma_k = u^{s-1-k}/(u-1)^{s-k}$  the pole at  $x=1$  disappears in the integral, since

$$\sum_{k=1}^{s-1} \gamma_k \frac{x^{k-1}}{(x-1)^k} = \frac{u^{s-1}}{(u-1)^{s-1}(x-u)} - \frac{x^{s-1}}{(x-1)^{s-1}(x-u)}. \quad (\text{B.18})$$

Therefore, with this choice of  $\gamma_k$ 's, and recalling (B.8), we have

$$B_{js}(u) = \frac{q!}{(q+j-1)! \alpha^{j-1}} \frac{u^{r+s-2}}{(u-1)^{s-1}} \sum_{m=0}^{r-1} \binom{m+q}{q} (m)_{j-1} \left(\frac{\alpha}{u}\right)^m. \quad (\text{B.19})$$

Similarly to (B.12), introduce matrix  $\tilde{B}(u)$ , with entries

$$\tilde{B}_{jk}(u) = \begin{cases} \tilde{A}_{jk} & k \neq s \\ \sum_{m=0}^{r-1} \binom{q+m}{q} (m)_{j-1} \left(\frac{\alpha}{u}\right)^m & k = s. \end{cases} \quad (\text{B.20})$$

We have

$$\det B(u) = \frac{(q!)^s}{\prod_{j=0}^{s-1} (q+j)!} \frac{u^{r+s-2}}{\alpha^{\frac{s(s-1)}{2}} (u-1)^{s-1}} \det \tilde{B}(u). \quad (\text{B.21})$$

In this case, the analogue of (B.14) is

$$\begin{aligned} \det \tilde{B}(u) &= \sum_{m_1, \dots, m_s=0}^{r-1} \prod_{k=1}^s \binom{m_k+q}{q} \\ &\quad \times \prod_{k=1}^{s-1} \binom{r+k-2-m_k}{k-1} \prod_{l<k} (m_k - m_l) \frac{\alpha^{m_1+\dots+m_s}}{u^{m_s}} \\ &= \frac{(-1)^{\frac{(s-1)(s-2)}{2}}}{\prod_{j=0}^{s-2} j!} \sum_{m_1, \dots, m_s=0}^{r-1} \prod_{k=1}^s \binom{m_k+q}{q} \prod_{l<k} (m_k - m_l) \\ &\quad \times \prod_{k=1}^{s-1} m_k^{k-1} \frac{\alpha^{m_1+\dots+m_s}}{u^{m_s}}. \end{aligned} \quad (\text{B.22})$$



Symmetrizing the summand with respect to permutations of  $m_1, \dots, m_s$  and substituting everything in (B.6), we get

$$\begin{aligned}
F_{N,r,s}(w) &= \frac{(q!)^s}{s! \prod_{j=0}^{s-1} (q+j)! \prod_{j=0}^{s-2} j!} \frac{(1-\alpha)^{s(s+q)}}{\alpha^{\frac{s(s-1)}{2}}} w^{r-1} \frac{u^{r+s-2}}{(u-1)^{s-1}} \\
&\times \sum_{m_1, \dots, m_s=0}^{r-1} \prod_{j=1}^s \binom{m_j+q}{q} \prod_{l < k} (m_k - m_l) \alpha^{m_1 + \dots + m_s} \\
&\times \sum_{p=1}^s (-1)^{p-1} \prod_{\substack{l < k \\ l, k \neq p}}^s (m_k - m_l) u^{-m_p}. \quad (\text{B.23})
\end{aligned}$$

Finally, rewriting the sum over  $p$  as a contour integral, we arrive at

$$F_{N,r,s}(w) = \frac{(q!)^s}{\prod_{j=0}^{s-1} (q+j)! \prod_{l=0}^s j!} \frac{(1-\alpha)^{s(N-r)}}{\alpha^{s(s-1)/2}} w^{r-1} I_{N,r,s}(u) \quad (\text{B.24})$$

where the quantity  $I_{N,r,s}(u)$  is defined in (3.6). Recalling (B.1), the statement of the Proposition 3.1, representation (3.4), immediately follows.

We also mention that (B.23) can be written as

$$F_{N,r,s}(w) = \frac{(q!)^s}{\prod_{j=0}^{s-1} (q+j)! \prod_{j=0}^{s-2} j!} \frac{(1-\alpha)^{s(s+q)}}{\alpha^{\frac{s(s-1)}{2}}} w^{r-1} \frac{u^{r+s-2}}{(1-u)^{s-1}} \det H, \quad (\text{B.25})$$

where the  $s \times s$  matrix  $H$  is

$$H_{jk} = \begin{cases} \sum_{m=0}^{r-1} \binom{m+q}{q} m^{j+k-2} \alpha^m & k \neq s \\ \sum_{m=0}^{r-1} \binom{m+q}{q} m^{j-1} \left(\frac{\alpha}{u}\right)^m & k = s. \end{cases} \quad (\text{B.26})$$

Note that, as  $w \rightarrow 1$  (that is,  $u \rightarrow 1$ ), the expected result (B.16) is reproduced from (B.25) upon taking into account that  $\det H$  has a zero of order  $(s-1)$  at  $u = 1$ .

### Appendix C. Arctic curve for Regime II, symmetric domain

Here we report explicit expression for the polynomial  $\mathcal{A}(z_1, z_2)$  describing the arctic curve, for the case  $Q = 0$  of the model in Regime II (symmetric L-shaped domain). The curve is given by the equation  $\mathcal{A}(z_1, z_2) = 0$  and it is of degree 6.

We first introduce properly scaled diagonal coordinates  $Z_1$  and  $Z_2$ , defining them by

$$z_1 = \sqrt{\alpha} Z_1, \quad z_2 = \sqrt{1-\alpha} Z_2. \quad (\text{C.1})$$

Recall that the original diagonal coordinates are defined by (4.18). Note, that in terms of the new coordinates the Arctic ellipse (2.9) just reads

$$Z_1^2 + Z_2^2 = 1. \quad (\text{C.2})$$

Next, we introduce the following parameterization for the scaling parameter  $R \in [1, R_c]$ :

$$R = \frac{1 + \sqrt{\alpha\beta}}{1 - \sqrt{\alpha\beta}}, \quad \beta \in [0, 1]. \quad (\text{C.3})$$

The meaning of this re-parameterization is to simplify further expressions for the coefficients of the arctic curve, making them polynomials in  $\alpha$  and  $\beta$ .

At last, we introduce coefficients  $C_{n_1 n_2}$  which describe the polynomial  $A(z_1, z_2)$  appearing in (4.22), in terms of the coordinates (C.1)

$$\mathcal{A}(z_1, z_2) = (1 - \alpha)^2 \alpha^6 \sum_{0 \leq n_1 + n_2 \leq 6} C_{n_1 n_2} Z_1^{n_1} Z_2^{n_2}. \quad (\text{C.4})$$

Note that because of the symmetry of the L-shaped domain under reflection with respect to the North-West/South-East diagonal, the arctic curve possesses the symmetry  $A(z_1, -z_2) = A(z_1, z_2)$ , that is, it depends only on even powers of  $z_2$ , i.e.,  $C_{n_1 n_2} = 0$  if  $n_2$  is odd ( $n_2 = 1, 3, 5$ ). This excludes 12 coefficients out of 28 in total, which describe a generic degree 6 curve.

The nonzero 16 coefficients have the following expressions:

$$\begin{aligned} C_{60} &= 64(1 - \alpha)^2 (1 - 2\alpha\beta + \alpha\beta^2)^2, \\ C_{50} &= 64(1 - \alpha)^2 [1 - (5 + 2\alpha)\beta + 18\alpha\beta^2 - 2\alpha(4 + 7\alpha)\beta^3 + 13\alpha^2\beta^4 - 3\alpha^2\beta^5], \\ C_{42} &= 128(1 - \alpha)^2 [1 + (2 - 6\alpha)\beta - 2(1 - \alpha - 3\alpha^2)\beta^2 + 2(1 - 3\alpha)\alpha\beta^3 + \alpha^2\beta^4], \\ C_{40} &= 16(1 - \alpha)[1 + \alpha - (22 - 18\alpha + 8\alpha^2)\beta + (41 + 13\alpha - 32\alpha^2 + 8\alpha^3)\beta^2 \\ &\quad - 4\alpha(36 - 25\alpha - \alpha^2)\beta^3 + \alpha(52 + 63\alpha - 85\alpha^2)\beta^4 - 6\alpha^2(13 - 11\alpha)\beta^5 \\ &\quad + (15 - 13\alpha)\alpha^2\beta^6], \\ C_{32} &= 128(1 - \alpha)^2 [(1 - 2(2 + \alpha)\beta - (4 - 18\alpha)\beta^2 + (4 - 6\alpha - 14\alpha^2)\beta^3 \\ &\quad - (4 - 13\alpha)\alpha\beta^4 - 2\alpha^2\beta^5], \\ C_{30} &= 32(1 - \alpha)(1 - \beta)[\alpha - (2 + 3\alpha + 2\alpha^2)\beta + (22 - 21\alpha + 19\alpha^2)\beta^2 \\ &\quad - \alpha(59 - 48\alpha + 19\alpha^2)\beta^3 + \alpha(22 + 18\alpha - 15\alpha^2)\beta^4 \\ &\quad - \alpha^2(28 - 17\alpha)\beta^5 + \alpha^2(5 - 3\alpha)\beta^6], \\ C_{24} &= 64(1 - \alpha)^2 [1 + (8 - 12\alpha)\beta - 2(4 - \alpha - 6\alpha^2)\beta^2 + 4\alpha(2 - 3\alpha)\beta^3 + \alpha^2\beta^4], \\ C_{22} &= -32(1 - \alpha)[1 + (12 - 26\alpha + 8\alpha^2)\beta - (15 - 3\alpha - 35\alpha^2 + 8\alpha^3)\beta^2 \\ &\quad - (22 - 96\alpha + 90\alpha^2 + 4\alpha^3)\beta^3 + (12 - 25\alpha - 35\alpha^2 + 63\alpha^3)\beta^4 \\ &\quad - 2\alpha(6 - 26\alpha + 23\alpha^2)\beta^5 - \alpha^2(6 - 7\alpha)\beta^6], \\ C_{20} &= 4(2 - \alpha)\alpha - 16\alpha(9 - 8\alpha + \alpha^2)\beta + 4(24 + 78\alpha - 36\alpha^2 - 42\alpha^3 + 4\alpha^4)\beta^2 \\ &\quad - 32(26 - 41\alpha + 64\alpha^2 - 45\alpha^3 + 3\alpha^4)\beta^3 \\ &\quad + 4(104 + 286\alpha - 438\alpha^2 + 322\alpha^3 - 204\alpha^4)\beta^4 \\ &\quad - 4\alpha(105 - 96\alpha + 33\alpha^2 - 28\alpha^3)\beta^5 + 2\alpha(41 + 102\alpha - 163\alpha^2 + 34\alpha^3)\beta^6 \\ &\quad - 8\alpha^2(16 - 20\alpha + 5\alpha^2)\beta^7 + \alpha^2(15 - 18\alpha + 4\alpha^2)\beta^8, \\ C_{14} &= 64(1 - \alpha)^2 [1 - (3 + 2\alpha)\beta - (8 - 18\alpha)\beta^2 + 2(4 - 2\alpha - 7\alpha^2)\beta^3 \\ &\quad - \alpha(8 - 13\alpha)\beta^4 - \alpha^2\beta^5], \\ C_{12} &= -32(1 - \alpha)[2 - \alpha - (6 + 3\alpha - 2\alpha^2)\beta - (16 - 58\alpha + 21\alpha^2)\beta^2 \\ &\quad + (14 - 20\alpha - 48\alpha^2 + 19\alpha^3)\beta^3 + (14 - 53\alpha + 78\alpha^2 - 4\alpha^3)\beta^4 \\ &\quad - (4 - 3\alpha - 16\alpha^2 + 36\alpha^3)\beta^5 + \alpha(4 - 17\alpha + 20\alpha^2)\beta^6 + \alpha^2(2 - 3\alpha)\beta^7], \\ C_{10} &= 4[4(1 - \alpha)^2\beta^2 + \alpha(1 - \beta)^4][\alpha - (4 - \alpha + 2\alpha^2)\beta + (28 - 30\alpha + 12\alpha^2)\beta^2 \\ &\quad - (8 + 22\alpha - 20\alpha^2)\beta^3 + \alpha(21 - 16\alpha)\beta^4 - \alpha(3 - 2\alpha)\beta^5], \end{aligned}$$

$$\begin{aligned}
C_{06} &= 256(1-\alpha)^3(1-\beta)\beta(1-\alpha\beta), \\
C_{04} &= 16(1-\alpha)^2[1 - (26-8\alpha)\beta + (41+30\alpha-8\alpha^2)\beta^2 - 4(1+21\alpha+\alpha^2)\beta^3 \\
&\quad - (8-30\alpha-41\alpha^2)\beta^4 + 2(4-13\alpha)\alpha\beta^5 + \alpha^2\beta^6], \\
C_{02} &= -8(1-\alpha)(1-\beta)[2-\alpha - (18-7\alpha+2\alpha^2)\beta + (32+16\alpha+\alpha^2+2\alpha^3)\beta^2 \\
&\quad + (24-138\alpha+29\alpha^2-10\alpha^3)\beta^3 + (10-29\alpha+138\alpha^2-24\alpha^3)\beta^4 \\
&\quad - (2+\alpha+16\alpha^2+32\alpha^3)\beta^5 + \alpha(2-7\alpha+18\alpha^2)\beta^6 + \alpha^2(1-2\alpha)\beta^7], \\
C_{00} &= (1-6\beta+\beta^2)[4(1-\alpha)^2\beta^2 + \alpha(1-\beta)^4]^2. \tag{C.5}
\end{aligned}$$

Note that the coefficients are polynomials in  $\alpha$  of the degree at most 4, and in  $\beta$  they are all, but  $C_{00}$ , of the degree at most 8; the latter is of the degree 10.

In the limit  $\beta \rightarrow 1$ , that is  $R \rightarrow R_c$ , the arctic curve factorizes onto two straight lines  $Z_1 = 1$ , the usual Arctic ellipse (C.2), as expected, and the point  $(Z_1, Z_2) = (1, 0)$  belonging to the Arctic ellipse:

$$A(z_1, z_2) \Big|_{\beta=1} = 64(1-\alpha)^6 \alpha^6 (Z_1 - 1)^2 (Z_1^2 + Z_2^2 - 1) [(Z_1 - 1)^2 + Z_2^2]. \tag{C.6}$$

In the limit  $\beta \rightarrow 0$ , that is  $R \rightarrow 1$ , the arctic curve factorizes onto two straight lines  $Z_1 = -1$ , and two Arctic ellipses of radii  $1/2$ :

$$\begin{aligned}
A(z_1, z_2) \Big|_{\beta=0} &= 16(1-\alpha)^4 \alpha^6 (Z_1 + 1)^2 \left[ \left( Z_2 - \frac{1}{2\sqrt{1-\alpha}} \right)^2 + Z_1^2 - \frac{1}{4} \right] \\
&\quad \times \left[ \left( Z_2 + \frac{1}{2\sqrt{1-\alpha}} \right)^2 + Z_1^2 - \frac{1}{4} \right], \tag{C.7}
\end{aligned}$$

as expected.

## References

- [1] V. E. Korepin and P. Zinn-Justin, *Thermodynamic limit of the six-vertex model with domain wall boundary conditions*, J. Phys. A **33** (2000), 7053–7066, arXiv:cond-mat/0004250.
- [2] P. Zinn-Justin, *Six-vertex model with domain wall boundary conditions and one-matrix model*, Phys. Rev. E **62** (2000), 3411–3418, arXiv:math-ph/0005008.
- [3] P. Zinn-Justin, *The influence of boundary conditions in the six-vertex model* (2002), arXiv:cond-mat/0205192.
- [4] N. Reshetikhin and K. Palamarchuk, *The 6-vertex model with fixed boundary conditions*, PoS **Solvay** (2006), 012, arXiv:1010.5011.
- [5] F. Colomo and A. G. Pronko, *The arctic curve of the domain-wall six-vertex model*, J. Stat. Phys. **138** (2010), 662–700, arXiv:0907.1264.
- [6] P. Bleher and K. Liechty, *Random Matrices and the Six-Vertex Model*, CRM monographs series, vol. 32, American Mathematical Society, Providence, RI, 2013.
- [7] N. Reshetikhin and A. Sridhar, *Integrability of limit shapes of the six-vertex model*, Commun. Math. Phys. **356** (2017), 535–563, arXiv:1510.01053.
- [8] N. Reshetikhin and A. Sridhar, *Limit shapes of the stochastic six-vertex model* (2016), arXiv:1609.01756.
- [9] N. Allegra, J. Dubail, J.-M. Stéphan, and J. Viti, *Inhomogeneous field theory inside the arctic circle*, J. Stat. Mech. **2016** (2016), 053108, arXiv:1512.02872.
- [10] A. Borodin, I. Corwin, and V. Gorin, *Stochastic six-vertex model*, Duke Math. J. **165** (2016), 563–624, arXiv:1407.6729.
- [11] E. Dimitrov, *Six-vertex models and the GUE-corners process*, Int. Math. Res. Notices (2018), in press, arXiv:1610.06893.
- [12] A. Granet, L. Budzynski, J. Dubail, and J.L. Jacobsen, *Inhomogeneous Gaussian free field inside the interacting Arctic curve*, arXiv:1807.07927.

- [13] W. Jockush, J. Propp, and P. Shor, *Random domino tilings and the arctic circle theorem*, arXiv:math/9801068.
- [14] H. Cohn, M. Larsen, and J. Propp, *The shape of a typical boxed plane partition*, New York J. Math. **4** (1998), 137–165, arXiv:math/9801059.
- [15] R. Cerf and R. Kenyon, *The low-temperature expansion of the Wulff crystal in the 3D Ising model*, Comm. Math. Phys. **222** (2001), 147–179.
- [16] A. Okounkov and N. Reshetikhin, *Correlation function of Schur process with application to local geometry of a random 3-dimensional Young diagram*, J. Amer. Math. Soc. **16** (2003), 581–603, arXiv:math/0107056.
- [17] P. L. Ferrari and H. Spohn, *Step fluctuations for a faceted crystal*, J. Stat. Phys. **113** (2003), 1–46, arXiv:cond-mat/0212456.
- [18] R. Kenyon and A. Okounkov, *Planar dimers and Harnack curves*, Duke Math. J. **131** (2006), 499–524, arXiv:math-ph/0311062.
- [19] R. Kenyon, A. Okounkov, and S. Sheffield, *Dimers and amoebae*, Ann. of Math. **163** (2006), 1019–1056, arXiv:math-ph/0311005.
- [20] R. Kenyon and A. Okounkov, *Limit shapes and the complex Burgers equation*, Acta Math. **199** (2007), 263–302, arXiv:math-ph/0507007.
- [21] T. K. Petersen and D. Speyer, *An arctic circle theorem for groves*, J. Comb. Theory. Series A **111** (2005), 137–164, arXiv:math/0407171.
- [22] B. Pittel and D. Romik, *Limit shapes for random square Young tableaux*, Adv. Appl. Math **38** (2007), 164–209, arXiv:math.PR/0405190.
- [23] P. Di Francesco and R. Soto-Garrido, *Arctic curves of the octahedron equation*, J. Phys. A: Math. Theor. **47** (2014), 285204, arXiv:1402.4493.
- [24] L. Petrov, *Asymptotics of random lozenge tilings via Gelfand–Tsetlin schemes*, Prob. Theor. and Rel. Fields **160** (2014), 429–487, arXiv:1202.3901.
- [25] D. Romik and P. Śniady, *Limit shapes of bumping routes in the Robinson–Schensted correspondence*, Random Struct. Algor. **48** (2016), 171–182, arXiv:1304.7589.
- [26] C. Boutillier, J. Bouttier, G. Chapuy, S. Corteel, and S. Ramassamy, *Dimers on rail yard graphs*, Ann. Inst. Henri Poincaré Comb. Phys. Interact. **4** (2017), 479–539, arXiv:1504.05176.
- [27] A. Bufetov and A. Knizel, *Asymptotics of random domino tilings of rectangular Aztec diamonds*, Ann. Inst. H. Poincaré Probab. Statist. **54** (2018), 1250–1290, arXiv:1604.01491.
- [28] P. Di Francesco and M.F. Lapa, *Arctic curves in path models from the tangent method*, J. Phys. A: Math. Theor. **51** (2018), 155202, arXiv:1711.03182.
- [29] P. Di Francesco and E. Guitter, *Arctic curves for paths with arbitrary starting points: a tangent method approach*, J. Phys. A: Math. Theor. (2018), arXiv:1803.11463. In press.
- [30] J.-M. Stéphan, *Return probability after a quantum quench from a domain wall initial state in the spin-1/2 XXZ chain*, J. Stat. Mech. Theory Exp. **2017** (2017), 103108, arXiv:1707.06625.
- [31] M. Collura, A. De Luca, and J. Viti, *Analytic solution of the domain wall nonequilibrium stationary state*, Phys. Rev. B **97** (2018), 081111, arXiv:1707.06218.
- [32] L. Cugliandolo, *Artificial spin-ice and vertex models*, J. Stat. Phys. **167** (2017), 499–514, arXiv:1701.02283.
- [33] V. E. Korepin, *Calculations of norms of Bethe wave functions*, Commun. Math. Phys. **86** (1982), 391–418.
- [34] F. Colomo and A. G. Pronko, *The limit shape of large alternating-sign matrices*, SIAM J. Discrete Math. **24** (2010), 1558–1571, arXiv:0803.2697.
- [35] F. Colomo, A. G. Pronko, and P. Zinn-Justin, *The arctic curve of the domain-wall six-vertex model in its anti-ferroelectric regime*, J. Stat. Mech. Theory Exp. (2010), L03002, arXiv:1001.2189.
- [36] F. Colomo and A. Sportiello, *Arctic curves of the six-vertex model on generic domains: the tangent method*, J. Stat. Phys. **164** (2016), 1488–1523, arXiv:1605.01388.
- [37] F. Colomo and A. G. Pronko, *Emptiness formation probability in the domain-wall six-vertex model*, Nucl. Phys. B **798** (2008), 340–362, arXiv:0712.1524.
- [38] K. Johansson, *Shape fluctuations and random matrices*, Commun. Math. Phys. **209** (2000), 437–476, arXiv:math/9903134.
- [39] A. G. Pronko, *On the emptiness formation probability in the free-fermion six-vertex model with domain wall boundary conditions*, J. Math. Sci. (N. Y.) **192** (2013), 101–116.
- [40] F. Colomo and A. G. Pronko, *Third-order phase transition in random tilings*, Phys. Rev. E **88** (2013), 042125, arXiv:1306.6207.

- [41] F. Colomo and A. G. Pronko, *Thermodynamics of the six-vertex model in an L-shaped domain*, Comm. Math. Phys. **339** (2015), 699–728, arXiv:1501.03135.
- [42] F. Colomo, A. G. Pronko, and A. Sportiello, *Generalized emptiness formation probability in the six-vertex model*, J. Phys. A: Math. Theor. **49** (2016), 415203, arXiv:1605.01700.
- [43] N. Elkies, G. Kuperberg, M. Larsen, and J. Propp, *Alternating-sign matrices and domino tilings*, J. Algebraic Combin. **1** (1992), 111–132; 219–234, arXiv:math/9201305.
- [44] J. Propp, *Generalized domino-shuffling*, Theoret. Computer Sci. **303** (2003), 267–301, arXiv:math/0111034.
- [45] J. Baik, T. Kriecherbauer, K. T.-R. McLaughlin, and P. D. Miller, *Discrete orthogonal polynomials: Asymptotics and applications*, Ann. of Math. Stud., vol. 164, Princeton University Press, Princeton, NJ, 2007.
- [46] M.R. Douglas and V.A. Kazakov, *Large  $N$  phase transition in continuum  $QCD_2$* , Phys. Lett. B **319** (1993), 219–230, arXiv:hep-th/9305047.
- [47] P. Zinn-Justin, *Universality of correlation functions of Hermitian random matrices in an external field*, Comm. Math. Phys. **194** (1998), 631–650, arXiv:cond-mat/9705044.

INFN, SEZIONE DI FIRENZE, VIA G. SANSONE 1, 50019 SESTO FIORENTINO (FI), ITALY  
*E-mail address:* colomo@fi.infn.it

STEKLOV MATHEMATICAL INSTITUTE, FONTANKA 27, 191023 ST. PETERSBURG, RUSSIA  
*E-mail address:* agp@pdmi.ras.ru

LIPN, AND CNRS, UNIVERSITÉ PARIS 13, SORBONNE PARIS CITÉ, 99 Av. J.-B. CLÉMENT,  
 93430 VILLETANEUSE, FRANCE  
*E-mail address:* Andrea.Sportiello@lipn.univ-paris13.fr